A Geometrical-Based Simulator for Target Recognition in High-Resolution SAR Images

Kan Tang, Xian Sun, Hao Sun, and Hongqi Wang

***Abstract*—Target recognition in high-resolution synthetic aperture radar (SAR) images is a challenging task. In this letter, a novel geometrical-based SAR image simulator is proposed to assist target recognition. Specifically, in addition to the using of Lamberitian-specular mixed model for single-bounce simulation, we propose a dihedral corner model for double-bounce simulation, which allows directly retrieving structure information from scattering patterns. In addition, a dihedral tracing technique is taken instead of ray tracing for double-bounce detection to reduce computation time. Also, a new primitive-by-primitive visualization approach which is well combined with our scattering model is proposed to obtain high efficiency. The efficiency of the simulator is demonstrated by the comparison between the simulated results and MiniSAR images and by the application in vehicle recognition.**

***Index Terms*—Dihedral corner, high-resolution images, synthetic aperture radar (SAR) image simulation, scattering, target recognition.**

I. Introduction

With the launch of new high-resolution synthetic aperture radar (SAR) missions, the following delivery of SAR images can reach spatial resolutions below 1 m [1]. Because of the increased resolution, many key geometric features of man-made targets can be identified from SAR images, which offers the opportunity of recognizing target based on geometric properties rather than radiometric properties [2]. However, SAR target recognition is still a tough task due to the high variation of image signatures caused by different target orientations, incidence angles, and resolutions. SAR simulation is one of the most potential tools to assist recognition. It not only permits investigating the scattering behaviors of different targets for interpretation purpose, but also provides simulated data for direct utilization.

Some simulators implement complete physical models, such as physical optics, physical theory of diffraction, finite-difference time domain method, and the integral equation method to get high radiometric quality [3]–[5]. While, in these models, various variables are needed to describe the interaction of signal with target, including detailed target structure, material properties, and surface roughness parameters, which limit the practical application [6]. Other simulators, which focus on geometrical quality rather than high radiometric quality, simplify the physical mechanism of scattering with diffusion-specular mixture model [6], [7]. This kind of simulator has already been successfully employed in high-resolution SAR images interpretation [1], building height retrieval, and 3-D reconstruction of urban structure [8]. It is demonstrated that simulators using simple scattering models have great potential in applications that utilize geometrical characteristics of the targets though they are less precise in radiometric simulation.

Scattering models are usually combined with ray tracing or rasterization techniques for scene visualization. Ray tracing approach visualizes the targets following geometrical optics [9], which considers the effects of multiple reflections, shadows, and occlusions automatically. However, it has a high computational load and is very time consuming. Rasterization, supported by state-of-the-art graphical processing units, can be used in real-time visualization [7]. In the rasterization approach, triangulated 3-D models are transformed into image coordinates, then rasterized into pixel fragments and processed separately. Shadows and occluded areas are determined by using shadow map. Multireflections, as well as double-bounce reflection, are not supported by rasterization. Therefore, an image-based ray-tracing technique has to be adopted additionally for double-bounce simulation.

In this letter, we are aiming at designing a fast and effective simulator to assist target recognition in high-resolution SAR images. Rather than high radiometric quality, we focus on the geometrical correctness of the simulation with simple scattering models. For the reason that geometry-based features are commonly used as discriminatory features in recognition application, e.g., the shape of target outlines, shadows, spatial distribution of dominant scattering centers [10]–[12].

For these purposes, we propose a new geometrical-based SAR image simulator which models the scattering behavior of targets in terms of their geometries and observation conditions. The novel contributions of the simulator are as follows. First, for radiometric calculation, in addition to the using of Lamberitian-specular mixed model for single-bounce simulation, we propose a dihedral corner model for double-bounce simulation. The model relates double-bounce effects with dihedral corners, which allows directly retrieving structure information from scattering patterns. In addition, a dihedral tracing technique is taken instead of ray tracing for double-bounce detection to reduce computation time. Second, a new primitive-by-primitive visualization approach is proposed. With this approach, geometry effects like shadow, occlude, layover can be modeled automatically. Also, this approach has the ability to represent the relative position of the visible parts of targets, which facilitates the searching of special target structure, particularly, dihedral corners. Thus, the visualization approach could be well combined with our dihedral corner model to obtain high efficiency.

Manuscript received September 5, 2011; revised December 31, 2011; accepted January 26, 2012. Date of publication March 19, 2012; date of current version May 29, 2012. This work was supported in part by the National Natural Science Foundation of China under Grant 41001285.

The authors are with Key Laboratory of Technology in Geo-spatial Information Processing and Application System, Chinese Academy of Sciences, Beijing 100190, China (e-mail: tangkan08@mails.gucas.ac.cn; sunxian0918@hotmail.com; sun.010@163.com; wiecas@sina.com).

Color versions of one or more of the figures in this paper are available online at http://ieeexplore.ieee.org.

Digital Object Identifier 10.1109/LGRS.2012.2187426

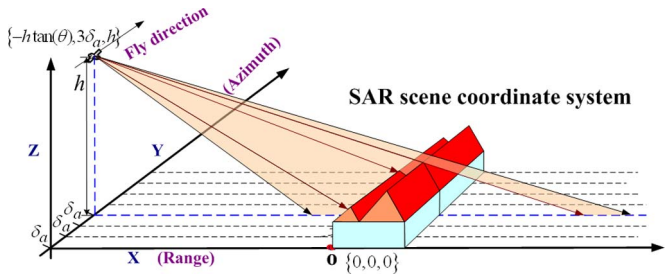

Fig. 1. Geometry of the simulator in the SAR scene space.

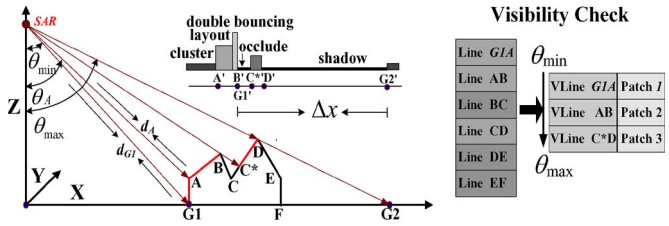

Fig. 2. Illumination scheme in the azimuth plane and the illustration of visibility check step, where the line G1A is represented by $L_{G1A} = [\theta_{\min}, \theta_A, d_{G1}, d_A]$.

The efficiency of the simulator has been demonstrated through two experiments: simulation of different targets in comparison to high-resolution MiniSAR images and application in vehicles recognition based on images from Moving and Stationary Target Acquisition and Recognition (MSTAR) data set.

II. Primitive-by-Primitive Visualization Approach

The geometry of the SAR imaging simulator in SAR scene coordinate is shown in Fig. 1, with the X-axis in range direction, Y-axis in azimuth direction, and Z-axis in height direction. Let θ denote the average incidence angle, δ_a and δ_{slr} be the azimuth and the slant range resolutions. h denotes the altitude of the sensor. The initial sensor position is given by $\vec{s} = \{-h\tan(\theta), 0, h\}$. The target model is set near the origin of the SAR scene coordinate system. It is assumed that the sensor sends and receives signals at a set of discrete locations where the coordinates in Y-axis are integer multiple of δ_a.Therefore, the SAR scene is divided into discrete azimuth cells. The visualization approach is processed separately within one azimuth resolution cell after another.

In Fig. 2, the illumination scheme in the azimuth (XZ) plane is presented. This plane is vertical to the azimuth direction with the coordinate which is integer multiple of δ_a in the positive Y-direction. Each primitive (normally triangle) contributed to this azimuth cell is represented by its intersection line with XZ plane. Hence, the visible primitive detection is simplified to a visibility check step to detect visible lines in XZ plane.

In the visibility check step, let $L = [\theta_h, \theta_t, d_h, d_t]$ denote the intersection line, where θ_h and θ_t are the vertical angles of the two line endpoints toward the sensor, d_h and d_t are the corresponding range distances. If a new line is about to be saved, its distance (d_h, d_t) is comparing against the already processed lines at its vertical angles range (θ_h, θ_t). Lines closer to the sensor replace the distance ones. As shown in Fig. 2, BC is blocked by AB. If a line is partly occluded, its endpoint moves along the line direction until there is no overlap in its new vertical angles region, e.g., in Fig. 2, line CD is partly occluded by AB. The endpoint C moves to C^* where the vertical angle of C^* is equal to that of B. The new line C^*D is saved instead of line CD.

After visibility check, all visible lines of this azimuth cell are automatically stored in sequence of their vertical angles, from $\theta_{\min}$ to $\theta_{\max}$.The corresponding visible primitives are called patches in this letter. Each patch is represented by $P = [d_h, d_t, \vec{n}]$, where $\vec{n}$ points to the normal of the patch, d_h/δ_{slr} and d_h/δ_{slr} determine the image coordinates of the patch at this range line. Patches are stored with the same order as lines. The storage order represents the relative positions of patches, which facilitates the tracing of special target structure, e.g., dihedral corner.

The computation of layover and shadow areas is an integral part of our approach. As shown in Fig. 2, patch AB and AG1 have the same range distances. Hence, the reflections from them can be incoherently summed up in $A'B'$ in the image coordinates which presents layover effect in image.

Two ground points G1 and G2, with the vertical angles $\theta_{\min}$ and $\theta_{\max}$, determine the position and size of the shadow areas. As shown in Fig. 2, in the image scene, the interruption of background signal starts from $G1'$ and extends for Δx.The shadow areas in the image coordinates start at the farther location of $G1'$ and the termination of target signal, end at $G2'$.

$$\Delta x = \left(\frac{h}{\cos\theta_{\max}} - \frac{h}{\cos\theta_{\min}}\right)/\delta_{slr}. \tag{1}$$

In the following section, the contributions of each patch including single-and double-bounce reflections are calculated by the geometrical-based radiometric model and finally assigned to pixels in the image coordinate according to their azimuth and slant range coordinates.

III. Geometrical-Based Radiometric Calculation

A. Single-Bounce Reflection

We introduce the Lambertian-specular model [1], [7] for single-bounce scattering calculation in our simulator. The model is simple, easy calculating, and with a few parameters. Moreover, the reflection strength is greatly depended on the target surface structure.

The Lambertian diffuse reflection intensity σ_d is defined as

$$\sigma_d = k_d\langle\vec{n}\cdot\vec{s}\rangle \tag{2}$$

where $\vec{s}$ is the vector pointing in the direction to the sensor, $\vec{n}$ is the normal vector of the patch, and k_d is the diffusion reflection coefficient. The specular reflection value σ_s can be simplified

$$\sigma_s = k_s\langle\vec{n}\cdot\vec{h}\rangle^p \tag{3}$$

where vector $\vec{h}$ is the bisection vector between the vector $\vec{s}$ pointing in the direction to the sensor and the direction vector $\vec{v}$ of the reflected ray, k_s is the specular reflectivity coefficient.

The overall single-bounce reflection strength of each patch is determined by summing up the diffuse reflection strength with the specular reflection strength.

B. Double-Bounce Reflection

The double-bounce effects are common in man-made structures in high-resolution SAR images and could be used as

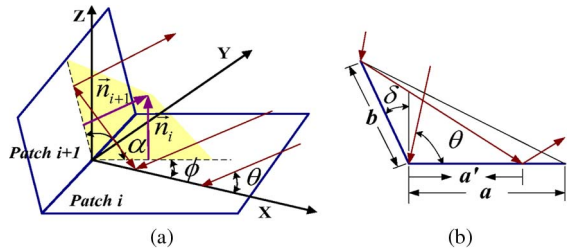

Fig. 3. (a) Geometry of a dihedral corner composed of two patches with aspect angle ϕ. (b) Geometry of a dihedral corner in azimuth plane.

important characteristics of targets. Generally, double-bounce effects which can be identified are caused by corner reflectors, e.g., the corner reflector between the front wall and its surrounding ground in buildings [13], particular parts like dihedrals and trihedrals in complex targets [12]. In this letter, we propose a dihedral corner model to simulate double-bounce reflections, under the assumption that main double-bounce effects are related to corner structures on the target surface. The image coordinates of double-bounce reflections are corresponding to the positions of the corner edges. Hence, the model allows directly retrieving corner reflectors from double-bounce effects. In addition, dihedral tracing could be used to detect double-bounce effects instead of ray tracing to reduce computation time. The tracing process is carried out by orderly calculating the internal angle of two adjacent patches stored in visualization. The parameters needed are the normal of the patches $\vec{n}_i$ and $\vec{n}_{i+1}$ [shown in Fig. 3(a)]. The internal angle α of a proper dihedral should not deviate much from orthogonality. Once a corner is detected, patches are traced both backward and forward to get the actual size of the corner. Also, the aspect angle of the corner ϕ can be computed from the normal of the patches.

In the literature, the scattering properties of the dihedral corner reflector are analyzed from different aspects. The scattering models for a dihedral corner in [14] and [15] show a dependence of its radar cross section on the corner size and internal angle. The relationship between strength of the double-bounce effect and the aspect angle of the dihedral corner is presented in [16]. Based on the previous research, we find the reflection strength of a dihedral has the following characteristics.

1) The scattering strength mainly depends on the internal angle, the aspect angle and the size of dihedral corner
2) The maximum double-bounce contribution occurs at the orthogonal dihedral reflector directly facing the sensor.
3) The reflection strength of a corner reflector decreases rapidly when the aspect angle increases or the internal angle deviates from orthogonal.

The relative strength of the double-bounce reflections σ_{db} is estimated by a simplified formula which describes the aforementioned characteristics

$$\sigma_{db} = k_{db} \frac{b^2 \cos^2(\tan^{-1} b/a) \cos^8 \phi}{(1 + A \sin \delta)^2} \tag{4}$$

where a, b are the corner sizes, $b^2 \cos^2(\tan^{-1} b/a)$ is the effect illuminated area of the corner, δ is the deviation angle of internal angle from orthogonal ($\delta \leq 15^\circ$), ϕ is the aspect angle, k_{db} is the double-bounce reflectivity coefficient.

Eventually, the effect of speckle is simulated by using a Rayleigh random number generator to produce a speckle image. The artificial noise-free image is multiplied by the speckle image pixel by pixel [17].

TABLE I
MINISAR DATA ACQUIRED ON 19TH MAY 2005

System Parameters	Numerical Value
Band	Ku
Resolution	4-inch
Swath Middle Range	3.3km
Incidence Angle	26^0-29^0
Center Frequency	16.8GHz

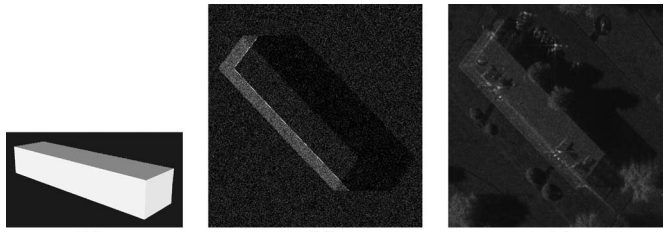

Fig. 4. (a) Three-dimensional model of a flat building. (b) Simulated result. (c) MiniSAR image.

IV. SAR SIMULATION-ASSISTED TARGET RECOGNITION

The SAR simulator can assist target recognition from two aspects. For one thing, a qualitative comparison between simulations and real SAR images could be useful for understanding the scattering patterns in multiple targets, and retrieving discriminatory geometrical information like target structures, special components from scattering effects. For another, the simulated data could be directly used in recognition arithmetic. For instance, in a model-based recognition approach [18], with the imaging condition and parameters being fixed to the test images, 3-D models of hypothesis types are imported and exported simulations are matched with test data, respectively. The target type is corresponding to the hypothesis type that has the highest match score.

In the following section, the performance of the simulator is evaluated from the both aspects through two experiments.

V. RESULTS

A. Simulation for Qualitative Analysis and Interpretation

We choose a flat roof building and a Lockheed C-130 Hercules military transport aircraft as two examples. The simulated results are compared with MiniSAR images. The acquisition parameters are given in Table I. The rotation angles of both examples have been estimated from the MiniSAR image. The exact values of reflectivity coefficients (k_d, k_s, k_{db}) used in radiometric models are empirically determined to achieve the best resemblance with the real data.

The 3-D model of the building [Fig. 4(a)] is composed of 12 primitives. The simulated result and the real SAR image are shown in Fig. 4(b) and (c). Geometrical features such as shadow and boundary are alike in the two images. The double-bounce reflection in the simulated image is clearly visible and lies at the right place comparing to the real image. Because rays are not tracing in scene space, double-bounce areas beyond the size of corners are not visible in our simulation.

The potentialities for complex target simulation have been shown by using C-130 as another example. The 3-D model shown in Fig. 5(b) is composed of 26593 primitives. The simulated result and actual image are shown in Fig. 5(c) and (d).The shadow areas and target outline in both images look

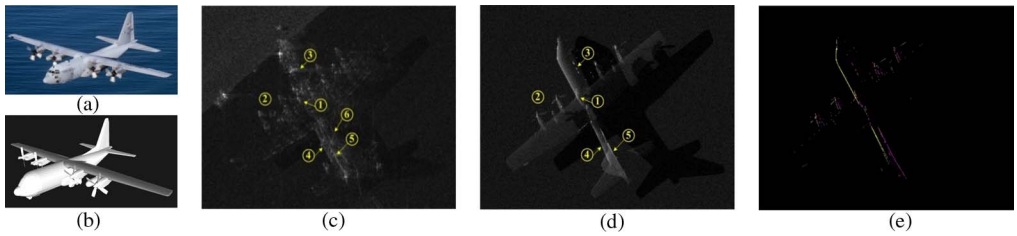

Fig. 5. (a) Photograph of the C-130. (b) Three-dimensional model of C-130. (c) MiniSAR image. (d) Simulated result. (e) Distributions of double bounce (mauve) and specular (yellow).

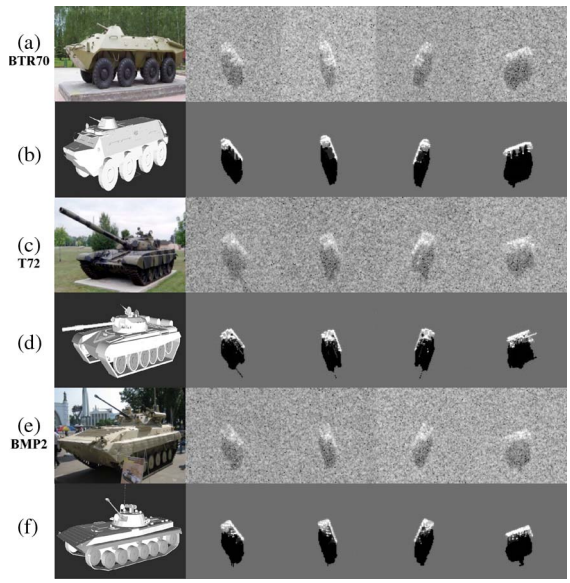

Fig. 6. (a), (b) MSTAR images and simulation results of BTR70, (c), (d) MSTAR images and simulation results of T72, and (e), (f) MSTAR images, and simulation results of BMP2. Aspect angles 18°, 34°, 111°, and 334°.

much alike. We marked several salient features on the MiniSAR image. Features 1, 2, 3 appear as strong scatterings distributing at different parts of plane. Concretely, feature 1 lies at the conjoint place of the wing and the body, feature 2 refers to the engines, and feature 3 points to the head. Features 4, 5, 6 appear as parallel linear structures at the backside of the plane.

Correspondingly, strong scattering features are marked on the simulated image to facilitate comparison. Though the 3-D model is only moderate compared to real plane [Fig. 6(a)], similarities (feature 1, 2, 3, 4, 5) are clearly visible in both actual image and the simulated result.

In Fig. 5(e), the double-bounce reflections and strong specular reflections are simulated separately to help explain scattering mechanisms of these visible features. The double-bounce reflections are colored mauve, and the strong specular reflections are colored yellow. The relative reflection intensities are disregarded to emphasize the geometrical distribution of scattering effects. Obviously, the linear feature 4 is the result of specular refection caused on the plane body. The linear feature 5, as a result of double-bounce reflection, can be retrieved to the corner formed by horizontal tail and vertical tail. Feature 3 is also the result of double-bounce reflection. The strong scatterings (feature 1) and (feature 2) are the results of both specular reflection and double-bounce refection. Since the features are further understood, they will be helpful in target recognition. Anyway, the above two examples exhibit the validity of our simulator to both simple and complex targets for analysis and interpretation.

The computation efficiency is also worth to be concerned. The simulation of the building takes 15 ms, with a personal computer (Intel R Petium(R) 4, CPU 3.06-GHz, 2-GB RAM and Microsoft Windows XP operating system).The simulation of C130 takes 3.937 s, 3.641 s for visualization and single-bounce reflection, 0.296 s for double-bounce reflection. Our simulator is faster than the ray tracing-based simulator [6] which takes 3 s to simulate simple gable-roof building. The rasterization-based simulator SARViz [7] implemented on GPU is faster at visualization. However, the computation time for double-bounce simulation is comparable to our simulator, highlighting the good performance of our simulator.

B. Application in Military Vehicles Recognition

We take 12 vehicle images of three types (BTR70, T72, and BMP2) at four different aspect angles (18°, 34°, 111°, and 334°) from the MSTAR data set for recognition test. The model-based approach is taken as the recognition arithmetic. The main simulation parameters including incidence angle 15°, resolution 0.3 m × 0.3 m, and mean range distance 4460 m are fixed to test images. All test images and simulations (without speckle noise in this case) are shown in Fig. 6.

For image matching, two methods are adopted [19]. The first is area-based match. It directly calculates the correlation between the actual SAR image and simulated images of hypothesis types (in our test, limited to BTR70, T72, and BMP2). The normalized cross-correlation coefficient (NCC) is used as match criterion, with the correlation images I_1 and I_2

$$NCC(I_1, I_2) = \frac{(I_1 - \bar{I}_1) \cdot (I_2 - \bar{I}_2)}{\|I_1 - \bar{I}_1\| \cdot \|I_2 - \bar{I}_2\|}. \tag{5}$$

The type of target $\hat{i}$ corresponds to the hypothesis type whose simulated result has the highest NCC

$$\hat{i} = \arg\max_i NCC(I, I_i). \tag{6}$$

The recognition results are shown in Table II. Area-based match is always affected by the speckle noise of the actual SAR images and particularly by the mismatch between the relative backscattering strengths of the simulated image and actual intensities of the real image. Still, the recognition results are all correct which demonstrates that the overall effect of the simulations is feasible.

A feature-based method is adopted as the second matching method. The shadow features are extracted from test images by using a median filter to reduce the affect of speckle noise and a threshold operator to segment the shadow areas from the

TABLE II
NCC COEFFICIENTS AND RECOGNITION RESULTS OF AREA-BASED MATCH AND FEATURE-BASED MATCH

Aspect Angle		Area-based			Recognize Type	Feature-based			Recognize Type	Ground Truth
		SBTR70	ST72	SBMP2		SBTR70	ST72	SBMP2		
18°	Test 1	**0.2333**	**0.1712**	**0.2101**	BTR70	**0.7330**	**0.5921**	**0.6759**	BTR70	BTR70
	Test 2	**0.3117**	**0.3389**	**0.3329**	T72	**0.6368**	**0.6593**	**0.6477**	T72	T72
	Test 3	**0.3223**	**0.3429**	**0.3746**	BMP2	**0.7445**	**0.6850**	**0.7701**	BMP2	BMP2
34°	Test 4	**0.2333**	**0.1661**	**0.2178**	BTR70	**0.7330**	**0.5763**	**0.7317**	BTR70	BTR70
	Test 5	**0.2930**	**0.3127**	**0.2964**	T72	**0.7683**	**0.7728**	**0.6606**	T72	T72
	Test 6	**0.1766**	**0.1891**	**0.3349**	BMP2	**0.6290**	**0.5278**	**0.7873**	BMP2	BMP2
111°	Test 7	**0.4041**	**0.3370**	**0.3952**	BTR70	**0.8401**	**0.7045**	**0.8206**	BTR70	BTR70
	Test 8	**0.3569**	**0.3847**	**0.3814**	T72	**0.7186**	**0.7305**	**0.7261**	T72	T72
	Test 9	**0.2669**	**0.3044**	**0.3970**	BMP2	**0.5789**	**0.7054**	**0.7579**	BMP2	BMP2
334°	Test 10	**0.2934**	**0.2453**	**0.2863**	BTR70	**0.7760**	**0.6605**	**0.7240**	BTR70	BTR70
	Test 11	**0.2626**	**0.2998**	**0.2875**	T72	**0.5964**	**0.7027**	**0.6702**	T72	T72
	Test 12	**0.2366**	**0.3002**	**0.3021**	BMP2	**0.7926**	**0.6877**	**0.8070**	BMP2	BMP2

Fig. 7. (a) Test image 7(BTR72), (b) the extracted shadow feature of Test image 7, and (c)–(e) shadow features of simulated BTR70, T72, and BMP2, aspect angle 111°.

test images. Then, the extracted shadow features are matched with the simulated ones. In Fig. 7(a) and (b), test image 7 and its shadow image are shown. The simulated shadow images of hypothesis types are shown in Fig. 7(c)–(e). The results are also shown in Table II.

Feature-based method is less affected by the speckle noise and the radiometric intensities. However, the match results depend on the effectiveness and stability of the feature extraction. In this case, feature-based match can correctly identify all targets. It implies that geometry features presented by our simulator carry the discriminatory information of a target class.

VI. CONCLUSION

In this letter, we propose a geometrical-based SAR image simulator to assist target recognition in high-resolution SAR images. A new primitive-by-primitive visualization procedure is used to deal with geometric effects, a Lambertian-specular mixture model is introduced to calculate the contribution of single-bounce reflection, and a dihedral corner model is adopted to simulate double-bounce effects.

The simulator is designed to present scattering behavior of targets in terms of their geometries and observation conditions Thus, the radiometric quality is constrained by disregarding radiometric effects related to material properties and surface roughness parameters. The dihedral corner model adopted for double-bounce simulation has limitation at ignoring the bounce between unconnected patches. Moreover, singles of higher reflection level, e.g., triple-bounce, are not modeled by our simulator.

Despite these drawbacks, the simulator is simple, efficient, and able to directly retrieve target structures from scattering patterns, making it helpful for target recognition. Two experiments are carried out to evaluate the simulator's performance. The results assess the effectiveness of the simulator in practical applications. Future work will focus on extending the dihedral tracing to unconnected patches and including the triple-bounce effects into our simulator.

REFERENCES

[1] S. Auer, S. Hinz, and R. Bamler, "Ray-tracing simulation techniques for understanding high-resolution SAR images," *IEEE Trans. Geosci. Remote Sens.*, vol. 48, no. 3, pp. 1445–1456, Mar. 2010.
[2] U. Soergel, U. Thoenessen, A. Brenner, and U. Stilla, "High resolution SAR data: New opportunities and challenges for the analysis of urban areas," *Proc. Inst. Elect. Eng.—Radar Sonar Navig*, vol. 153, no. 3, pp. 294–300, Jun. 2006.
[3] J. M. Rius, M. Ferrando, and L. Jofre, "High-frequency RCS of complex radar targets in real-time," *IEEE Trans. Antennas Propag.*, vol. 41, no. 9, pp. 1308–1319, Sep. 1993.
[4] J. Delliere, H. Maître, and A. Maruani, "SAR measurement simulation on urban structures using a FDTD technique," in *Proc. Urban Remote Sens. Joint Event*, 2007, pp. 1–8.
[5] F. Xu and Y.-Q. Jin, "Imaging simulation of polarimetric SAR for a comprehensive terrain scene using the mapping and projection algorithm," *IEEE Trans. Geosci. Remote Sens.*, vol. 44, no. 11, pp. 3219–3234, Nov. 2006.
[6] D. Brunner, G. Lemoine, L. Bruzzone, H. Bruzzone, and H. Greidanus, "Radar imaging simulation for urban structures," *IEEE Geosci. Remote Sens. Lett.*, vol. 8, no. 1, pp. 68–72, Jan. 2011.
[7] T. Balz and U. Stilla, "Hybrid GPU based single and double bounce SAR simulation," *IEEE Trans. Geosci. Remote Sens.*, vol. 47, no. 10, pp. 3519–3529, Oct. 2009.
[8] D. Brunner, G. Lemoine, L. Bruzzone, and H. Greidanus, "Building height retrieval from VHR SAR imagery based on an iterative simulation and matching technique," *IEEE Trans. Geosci. Remote Sens.*, vol. 48, no. 3, pp. 1487–1504, Mar. 2010.
[9] A. S. Glassner, *An Introduction to Ray Tracing*, 9th ed. San Francisco, CA: Morgan Kaufmann, 2002.
[10] L. P. Nicoli and G. C. Anagnostopoulos, "Shape-based recognition of targets in synthetic aperture radar images using elliptical fourier," *Proc. SPIE*, vol. 6967, p. 696 70G , 2008.
[11] M. Jahangir, D. Blacknell, C. P. Moate, and R. D. Hill, "Extracting information from shadows in SAR imagery," in *Proc. ICMV*, 2007, pp. 28–29.
[12] G. Margarit, J. J. Mallorqui, and X. F. Abregas, "Single-pass polarimetric SAR interferometry for vessel classification," *IEEE Trans. Geosci. Remote Sens.*, vol. 45, no. 11, pp. 3494–3502, Nov. 2007.
[13] D. Brunner, L. Bruzzone, A. Ferro, and G. Lemoine, "Analysis of the reliability of the double bounce scattering mechanism for detecting buildings in VHR SAR images," in *Proc. IEEE RadarCon*, Pasadena, CA, 2009, pp. 1–6.
[14] E. F. Knott, "RCS reduction of dihedral corners," *IEEE Trans. Antennas Propag.*, vol. 25, no. 3, pp. 406–409, May 1977.
[15] W. C. Aanderson, "Consequences of nonorthogonality on the scattering properties of dihedral reflectors," *IEEE Trans. Antennas Propag.*, vol. AP-35, no. 10, pp. 1154–1159, Oct. 1987.
[16] Y. Dong, B. Forster, and C. Ticehurst, "Radar backscatter analysis for urban environments," *Int. J. Remote Sens*, vol. 18, no. 6, pp. 1351–1364, 1997.
[17] R. Bolter, M. Gelautz, and F. Leberl, "SAR speckle simulation," *Int. Arch. Photogramm. Remote Sens*, vol. 21, no. B2, pp. 20–25, 1996.
[18] R. Hummel, "Model-based ATR using synthetic aperture radar," in *Proc. IEEE Int. Radar Conf.*, 2000, pp. 856–861.
[19] D. Brunner, G. Lemoine, and L. Bruzzone, "Height estimation of man-made structures using hybrid VHR optical and SAR imagery," in *Proc. EARSeL Joint Workshop, Remote Sens.—New Challenges High Resolution*, C. Juergens, Ed., 2008, pp. 186–193.